

RESEARCH PAPER

In-situ Synthesis and Characterization of Reduced Graphene Oxide–Ag Nanocomposites

Mohit Sharma ^{1,2} *, Manoj Kumar Patra ¹ and S.K.Jain ³

¹ Defence Laboratory, Jodhpur-342011, India

² Jai Narain Vyas University, Jodhpur-342001, India

³ Formerly in Defence Laboratory, Jodhpur-342011, India

ARTICLE INFO

Article History:

Received 17 January 2019

Accepted 04 June 2019

Published 01 July 2019

Keywords:

Ag

DMF

Liquid Exfoliation

Luminescence

Nanocomposite

Reduced Graphene Oxide

ABSTRACT

Reduced graphene oxide(rGO)–silver(Ag) nanocomposites have been prepared by using solution based facile one-pot synthesis process. The reaction process involves high-temperature liquid-phase exfoliation of graphite oxide and silver acetate in presence of N-N'dimethylformamide (DMF) solvent, resulting in simultaneous formation of rGO as well as Ag nanoparticles. Different nanocomposites have been prepared by varying the ratio of graphite oxide and Ag ions during the reaction. The crystal structure, chemical structure, morphology, and photoluminescence properties have been investigated by using powder X-Ray Diffraction (XRD), Raman spectroscopy, Fourier Transform Infra-Red spectroscopy (FTIR), Atomic Force Microscopy (AFM), Scanning Electron Microscopy (SEM), and Photo Luminescence (PL) spectroscopy techniques respectively. The microscopic studies reveal a uniform distribution of silver nanoparticles of size ~ 200 nm on to graphene layers. Further, average defect distance in the graphene layers was estimated to be 11 nm from Raman peak ratio in these nanocomposites. These nanocomposites showed luminescent emission around 410 nm and intensity of emission enhanced significantly for the nanocomposites comprising more silver nanoparticles, which may be due to resonant energy transfer between Ag metal and rGO.

How to cite this article

Sharma M, Kumar Patra M, Jain SK. In-situ Synthesis and Characterization of Reduced Graphene Oxide–Ag Nanocomposites. J Nanostruct, 2019; 9(3): 547-555. DOI: 10.22052/JNS.2019.03.016

INTRODUCTION

Graphene based composites have attracted attention of the research community due to their numerous potential applications in the field of water purification, energy storage, photocatalysis, sensors, biological applications etc. [1–6]. Among these, graphene metal based composites are a matter of interest due to the presence of nano-sized metals within graphene layers. They provide interesting physical properties arising from both graphene layers and nanoparticles. These composites also provide the opportunity for tailoring the composite properties by varying the metal ion content within composites. Ag nanoparticles have been widely explored for their

use in different applications viz. sensing, photonics, antimicrobial coatings, and water purification applications etc. [7-11]. Recently, graphene-Ag nanoparticle-based nanocomposites have been reported to exhibit improved properties for their applications in catalysis, antibacterial, biomolecule detection etc. [12-15]. However, the applications of these nanocomposites are restricted due to the limitation of material quality as it is highly dependent on preparatory methods. Further, uniform dispersion of nanoparticles in graphene is an issue which affects the functional properties of the nanocomposites. Considering the importance of such nanocomposites, it will be interesting to establish a facile and economic method to prepare

* Corresponding Author Email: mohitsharma@dl.drdo.in

such nanocomposites with high yield and quality for practical uses.

In the preparatory side, different synthesis methods viz. hydrothermal, microwave-assisted reduction, thermal annealing etc. have been utilized for the preparation of graphene-Ag nanoparticle based nanocomposites [15-17]. In these methods, several reducing agents such as NaBH_4 , citric/ascorbic acid, and L-arginine are used for reduction of AgNO_3 precursor [8,18-20]. Similarly, N-N'dimethylformamide (DMF) solvent has also been reported to act as a reducing agent and used for reduction of AgNO_3 , AgClO_4 , CH_3COOAg to Ag metal [21-22] and for reduction of graphene oxide by high-temperature process [23]. There are several reports in which authors have utilized DMF as a solvent for dispersion and exfoliation of graphite oxide to prepare graphene oxide sheets [24, 25]. Yang et al. carried out reduction of AgNO_3 onto graphene oxide in DMF through sonochemical route [26]. In most of these methods, various complex steps are involved in the formation of the nanocomposites which are time consuming. Therefore, preparation of such nanocomposites always becomes challenging to obtain quality materials.

To the best of our knowledge, no such reports are available for simultaneous formation of rGO from graphite oxide and Ag nanoparticle in a single step to obtain rGO-Ag nanocomposites. In this paper, we report facile, one-pot synthesis method for preparation of rGO-Ag nanocomposite, wherein exfoliation of graphite oxide to form rGO and reduction of Ag precursors to Ag takes place simultaneously. The simultaneous formation of rGO layers and Ag particles offers advantages for the homogeneous distribution of Ag onto rGO

layers, leading to better nanocomposite materials. The concentration of Ag ions is varied during the reaction process to obtain nanocomposites comprising different concentrations of Ag particles. The as-synthesized materials have been characterized by using XRD, Raman, FTIR, AFM, SEM, and PL techniques.

MATERIALS AND METHODS

All chemicals used in synthesis were of laboratory grade. Graphite oxide was synthesized from graphite by modified Hummer's method [27, 28]. For preparation of graphite oxide, 230 mL of 18M H_2SO_4 was taken in a beaker (5 L capacity) and cooled to 5 °C using an ice bath. To this reactant, a mixture of powdered flake graphite (10 g) and NaNO_3 (5 g) was added gradually under constant stirring. Subsequently, addition of KMnO_4 (30 g) was carried out slowly while maintaining the temperature below 10 °C. The temperature of reaction mixture was then allowed to increase up to 40 °C by removal of the ice bath. The reaction mixture was then kept stirring for 1 hour till it turned to grey-brown paste. Further, 460 mL of Distilled Water (D.W.) was gradually added to this paste, allowing the mixture temperature rise up to 95 °C. The reaction mixture was diluted with 1.4 L of D.W. and further treated with 20 mL of 30% H_2O_2 . The resultant brown solution was then vacuum filtered and washed with D.W. Finally, the product was treated with 100 mL of dilute HNO_3 (5M concentration) to remove residual metal ions from the product, again washed with D.W., and dried in a vacuum oven at 50 °C.

For the nanocomposites preparation, graphite oxide and silver acetate were taken in predefined ratios and homogenized in a mortar pestle. The

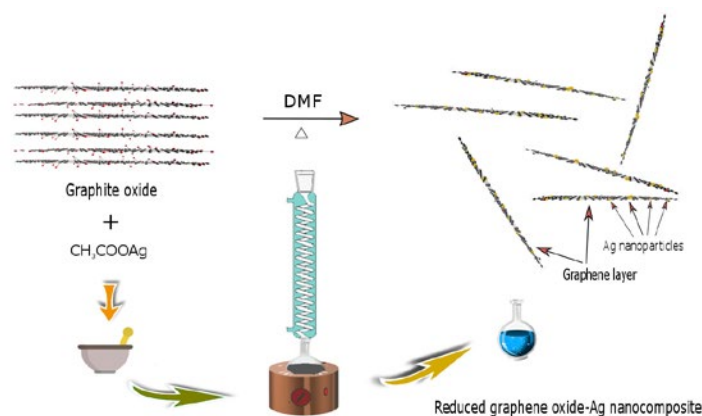


Fig. 1. Schematic of one pot synthesis of rGO-Ag nanocomposite

Table 1: Sample nomenclature and precursor quantities for nanocomposites

Sample Code	Graphite Oxide	Silver Acetate (in mili moles)
S ₀	1.5 g	0
S ₁	1.5 g	2.5
S ₂	1.5 g	5
S ₃	1.5 g	10
S ₄	1.5 g	20

mixture was then transferred to a round bottom flask containing 100 mL DMF solvent and refluxed at 150 °C for 4 hours. Subsequently, the product was cooled to ambient temperature, filtered, washed repeatedly by methanol to remove residual solvent. Finally, the obtained product was dried in a vacuum oven at 60 °C. Schematic of the nanocomposite formation is shown in Fig. 1. In this process, the solvent DMF acts as an exfoliation medium to form graphene oxide from graphite oxide as well as the reducing agent to facilitate simultaneous formation of rGO and Ag nanoparticles. The ratio of graphite oxide and silver acetate precursors are varied to obtain different nanocomposite materials as given in Table 1.

Powder XRD characterizations of the nanocomposites were carried out using a Philips X'Pert Pro system using Cu K_α¹ ($\lambda=1.54 \text{ \AA}$) radiation to investigate the crystalline phases present in the samples. Raman spectra of the samples were recorded using an Avalon Raman Microscope R3-532 using argon ion laser ($\lambda=532 \text{ nm}$). FTIR spectra were recorded using JASCO 610 FTIR spectrometer

using KBr pellets in transmission mode. The morphological studies of the samples have been carried out using an AFM, NT-MDT Solver TS 150. The samples were prepared by spraying a colloidal solution of the nanocomposites on a freshly cleaved mica substrate. SEM studies were carried out using Carl Zeiss SMT Ltd, EVO-MA 15 instrument. For these, the samples were spread onto a conductive carbon tape. A Spectrofluorometer, JASCO FP-6500, employing 150W Xenon flash lamp and R938 Hamamatsu PMT detector was used for room temperature PL studies of samples.

RESULTS AND DISCUSSIONS

Fig. 2 shows the XRD spectra of as-prepared rGO and graphite oxide. From the figure, it is seen that diffraction peak appears at lower 2θ angle 10.9° due to (001) plane of graphite oxide. The interlayer distance of graphite oxide was calculated using Bragg's law, $n\lambda=2.d.\sin\theta$, where n =order of diffraction, $\lambda=1.54 \text{ \AA}$ (wavelength of X-ray), d =inter-planer distance, and θ =angle of diffraction. The interlayer distance is found to be $\sim 4.07 \text{ \AA}$ for this peak which is greater than that of graphite (3.35 \AA). However, after exfoliation in DMF, this peak completely disappeared and broad diffraction peaks appeared at 2θ angle 25° , 43° , and 72.7° corresponding to (002), (100) and (110) planes of rGO layers respectively (sample S₀). The peaks confirm the formation of rGO during liquid phase exfoliation of graphite oxide in DMF. From Bragg's law calculation, the interlayer distance is

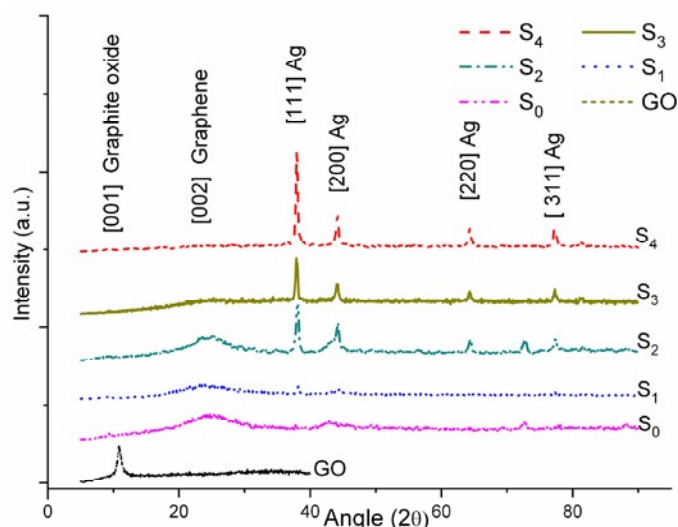


Fig. 2. X-ray diffractogram of Graphite oxide, rGO and rGO–Ag nanocomposites

found to be $\sim 3.56 \text{ \AA}$ for (002) diffraction peak for rGO. The average stacking height of graphene layers was calculated by using Scherrer's equation $D = \frac{K\lambda}{B \cdot \cos \theta}$ where D=Crystallite size, $\lambda=1.54 \text{ \AA}$ (wavelength of X-ray), B=full width of peak at half maxima, K=constant (0.89), and θ =angle of diffraction. The average stacking height is calculated to be 1.34 nm for (002) diffraction peak. Similarly, for estimation of the lateral size of rGO sheets, diffraction angle for peak (110) and $K=1.84$ were utilized in Scherrer's equation [29]. The lateral size of rGO in the present synthesis was found to be $\sim 18 \text{ nm}$. The ratio of stacking height to interlayer distance in rGO sample

comes out to be 3.76, indicating average stacking of ~ 4 graphene sheets. Further, in case of rGO-Ag nanocomposites (S_1 to S_4 samples), additional diffraction peaks appeared in XRD spectra at 2θ angles of 38.0° , 44.1° , 64.3° , 77.3° , corresponding to (111), (200), (220), and (311) planes of face-centred cubic structure of pure Ag respectively (JCPDS file no. 04-0783). However, with an increase of Ag precursor content in nanocomposites, the broad peaks due to rGO get subdued, probably due to prominent peaks of crystalline Ag. The intensity of XRD peaks of Ag also increased with increase of Ag content in the samples.

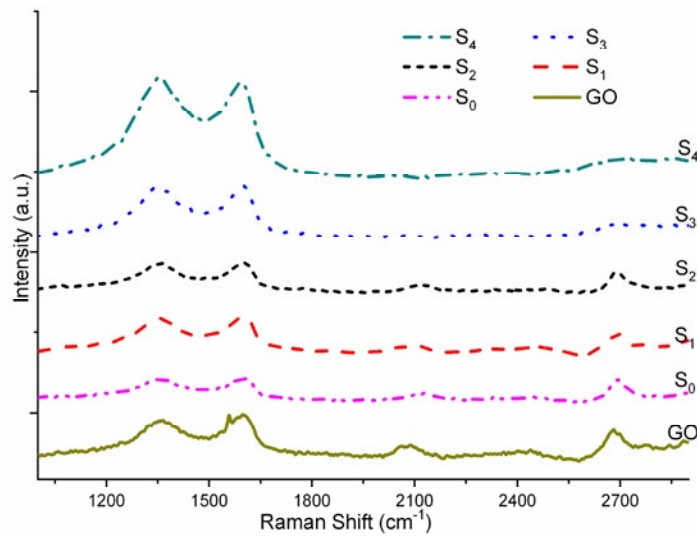


Fig. 3. Raman spectra of rGO-Ag nanocomposites

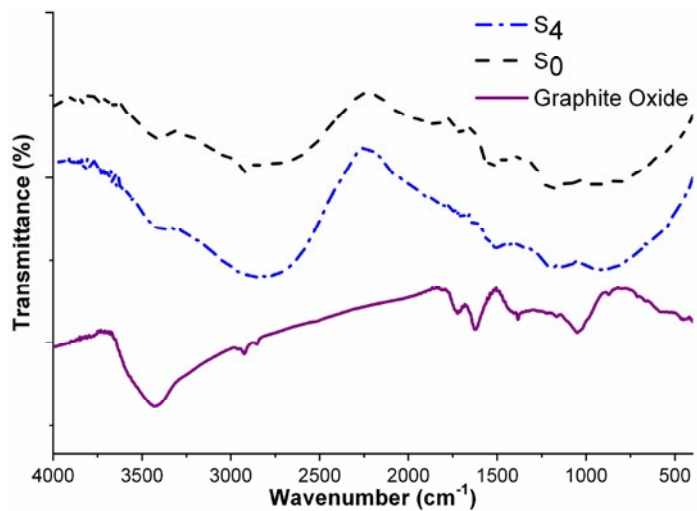


Fig. 4. FTIR spectra of graphite oxide, reduced graphene oxide and rGO-Ag nanocomposites

Raman spectroscopy has been widely used for characterization of graphene-based materials [30-32]. The Raman spectra of nanocomposites are shown in Fig. 3. All the spectra show two Raman scattering bands due to graphene layers. The G band, corresponding to first order E_{2g} scattering, is seen at $\sim 1595 \text{ cm}^{-1}$. The observed upward shift as compared to G band scattering of graphitic structures ($\sim 1585 \text{ cm}^{-1}$) in the present study, is attributed to stress in the graphene layer [33, 34]. Similarly, another peak is observed at $\sim 1355 \text{ cm}^{-1}$ corresponding to D band, attributed to A_{1g} mode of graphene layer [35]. A high ratio of D/G band intensities gives an indication of reduced sp^2 domains [36]. The intensity ratio of D and G peaks, (I_D/I_G) were calculated from the spectra and found to be $\sim 0.94, 0.96, 0.97, 0.95,$ and 1.05 for samples S_0 to S_4 respectively. There is a possibility that defects get introduced in rGO sheets during synthesis as well as by doping with metals etc. [37]. In view of this, the average distance between defects in graphene sheets needs to be estimated. The average distance between defects L_D related to (I_D/I_G), can be expressed by the following equation [38]:

$$L_D^2 (nm) = 1.8 \times 10^{-9} \lambda_L^4 \times \frac{I_D}{I_G} \quad (1)$$

where $\lambda_L = 514 \text{ nm}$. Using the above relation, the average defect distance is estimated to be $11.56 \text{ nm}, 11.44 \text{ nm}, 11.38 \text{ nm}, 11.5 \text{ nm},$ and 10.94 for samples S_0 to S_4 respectively. It is noted here that

the increased doping of Ag in rGO reduces the average distance between defects. Further, the peak at $\sim 2695 \text{ cm}^{-1}$ is attributed to 2D band of rGO layers [39]. 2D peak intensity gets significantly reduced with the increase of Ag content in nanocomposites. This is in agreement with the earlier study carried out by Das et al. wherein they observed the decrease in I_{2D}/I_G ratio with an increase in doping of graphene layer [40].

FTIR spectra of the samples are shown in Fig. 4. For graphite oxide, the broad absorption band $\sim 3440 \text{ cm}^{-1}$ is attributed to O-H stretching vibration of hydroxyl groups. Similarly, peaks $\sim 1627 \text{ cm}^{-1}$ and 1725 cm^{-1} are attributed to $>C=O$ stretching of carbonyl groups. The peak $\sim 1052 \text{ cm}^{-1}$ is observed due to C-O stretching in hydroxyl groups. These peaks are not observed in the rGO as well as rGO-Ag nanocomposites. The above observations indicate that graphite oxide is exfoliated to graphene oxide and subsequently reduced to rGO in presence of DMF solvent [23].

AFM micrograph taken on the nanocomposite sample S_4 , in phase contrast mode, reveals the dispersion of Ag particle over rGO matrix (Fig. 5). The size of Ag metal particles is observed to be $\sim 230 \text{ nm}$. Further, SEM micrographs taken on the nanocomposite samples S_0 and S_4 are shown in Fig. 6. From the micrographs, layer morphology is observed for pure rGO (Fig. 6a), whereas Ag particle impregnated over rGO are observed for sample S_4 (Fig. 6b). The shape of the Ag particles is found to be spherical with size $\sim 200 \text{ nm}$.

PL spectra of the samples have been recorded

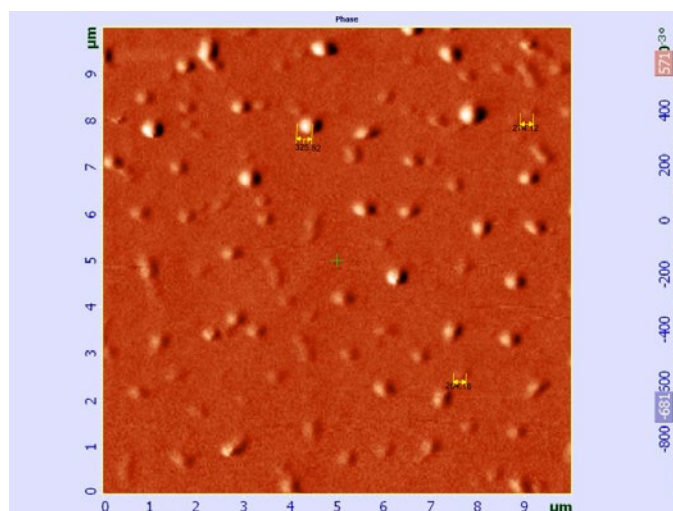


Fig. 5. Atomic Force Micrograph of rGO-Ag nanocomposite (Sample S_4)

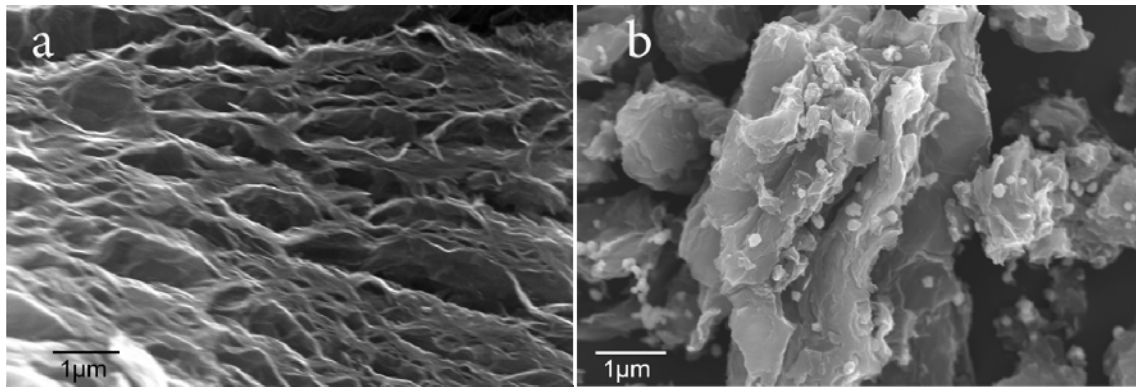


Fig. 6. Scanning Electron Micrograph of (a) rGO (sample S_0) and (b) rGO-Ag nanocomposite (Sample S_4)

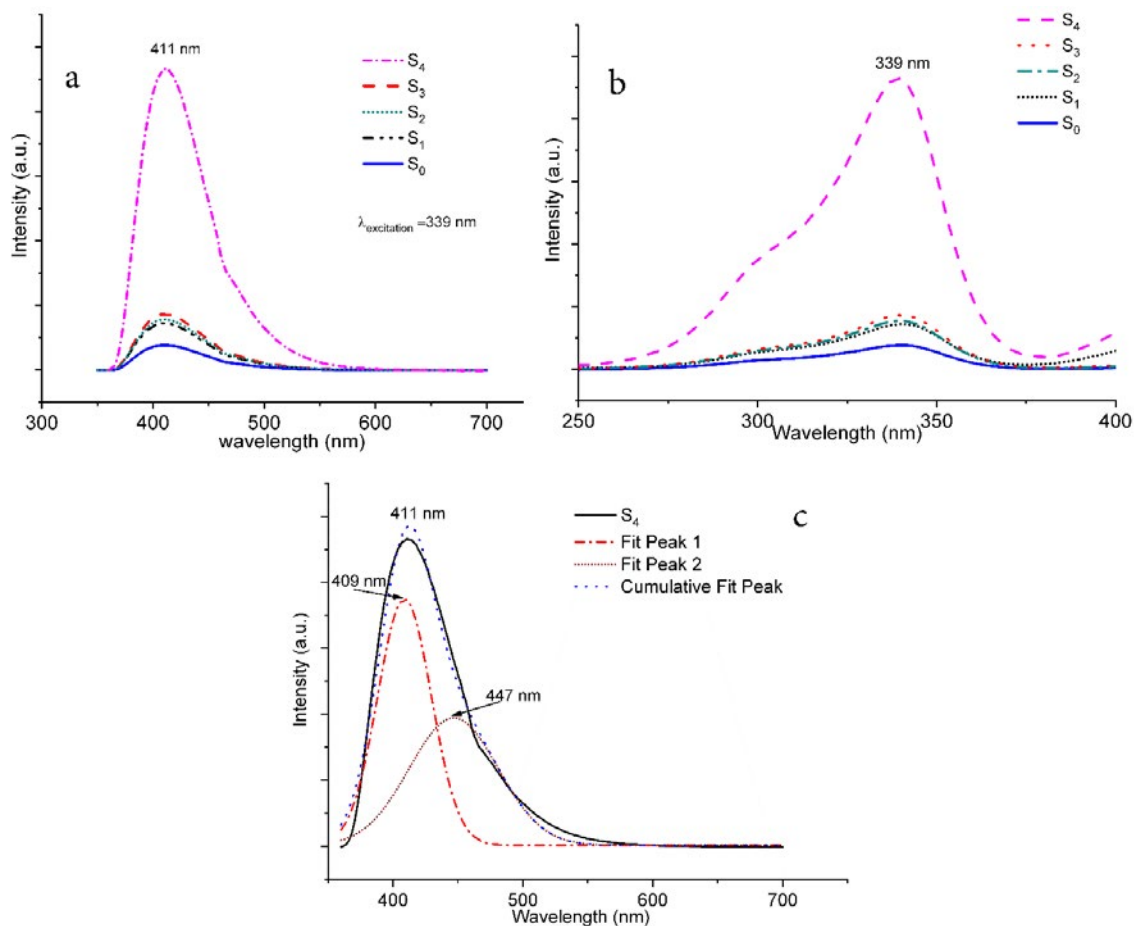


Fig. 7. Photo Luminescence spectra of rGO-Ag nanocomposites (a) Emission spectra, (b) Excitation spectra, (c) Deconvolution of emission spectrum

to investigate their luminescence properties. Fig. 7 shows emission and excitation spectra for the as-synthesized nanocomposites. As evident from the Fig. 7a, broad emission at ~ 411 nm, corresponding to band gap of 3.02 eV is seen

for the nanocomposites. The corresponding excitation wavelength maxima at ~ 339 nm (3.66 eV) can be seen for all the nanocomposites (Fig. 7b). Interestingly, we have observed a six-fold increase in the intensity of PL emission for sample

S_4 in comparison to other samples. Similarly, the intensity of excitation spectra in sample S_4 is found to be high as compared to other samples indicating more energy absorption by sample comprising more Ag metal particles. The rGO sample (S_0) shows emission with lesser intensity. The similar blue emission from the chemically derived graphene oxide has been observed by earlier authors [41, 42].

Gan et al. have reported PL properties of solvothermally reduced graphene oxide in DMF and observed a multi peak emission from rGO upon excitation with 340 nm wavelength, and corresponding blue emission spectrum was fitted to show two emission peaks [43]. The genesis of PL in graphene has been attributed to structural defects and/or oxygen containing functional groups in general. Particularly, the blue emission occurs due to localized sp^2/sp^3 regions, where electron-hole recombinations take place [44, 45]. Chien et al. have noted in their study that among different rGO samples, blue PL was exhibited by highly reduced graphene [46].

In our study, the enhanced peak emission intensity was observed for the nanocomposite comprising more Ag particle content. The broad emission peak of sample S_4 was deconvoluted into two constituent peaks at 409 nm and 447 nm respectively, by Gaussian fitting (Fig. 7c). Gan et al. have noticed that longer wavelength in the deconvoluted emission spectra appeared due to the presence of functional groups/metal ions on the graphene surfaces [43]. Long wave PL enhancement has been attributed to resonant energy transfer between metal and sp^2 domains of rGO [47]. In another study, Wang et al. have shown the possibility of PL enhancement in graphene quantum dots by Ag nanoparticles [48].

Although there are an immense amount of reports on PL emission property of Ag nano metal/nano clusters, the underlying mechanism behind PL is different and depends on various factors like size, ligands, dispersion medium, particle surface topography etc. In the present study, excitation of electrons takes place from occupied d bands above the Fermi level and subsequent electron-phonon and hole-phonon scattering processes. This leads to an energy loss. Finally, PL radiative recombination of electron from occupied sp^2 level with hole takes place to give emission [49, 50]. From above-mentioned observations, the PL emission from the nanocomposites is attributed to

rGO as well as to the presence of Ag metal in the nanocomposites. Further, enhanced PL emission intensity for sample S_4 may be due to the presence of more Ag particles resulting in resonant energy transfer between metal and rGO.

CONCLUSION

A facile, one-pot synthetic route has been demonstrated for preparation of rGO–Ag nanocomposites. In-situ exfoliation of graphite oxide and reduction of Ag ions into Ag has been confirmed by XRD studies. The Ag nanoparticles are found uniformly distributed on rGO layers. The nanocomposites containing more Ag show strong blue PL emission ~ 410 nm. These nanocomposites may be useful for water purification, antibacterial and bio-molecule detection applications.

ACKNOWLEDGEMENTS

The authors are grateful to Director, Defence Laboratory, Jodhpur for necessary permission and encouragements.

CONFLICT OF INTEREST

The authors declare that there are no conflicts of interest regarding the publication of this manuscript.

REFERENCES

1. Sreeprasad TS, Maliyekkal SM, Lisha KP, Pradeep T. Reduced graphene oxide–metal/metal oxide composites: Facile synthesis and application in water purification. *Journal of Hazardous Materials*. 2011;186(1):921-31.
2. Huang X, Qi X, Boey F, Zhang H. Graphene-based composites. *Chem Soc Rev*. 2012;41(2):666-86.
3. Tan C, Huang X, Zhang H. Synthesis and applications of graphene-based noble metal nanostructures. *Materials Today*. 2013;16(1-2):29-36.
4. Shao Y, Wang J, Wu H, Liu J, Aksay IA, Lin Y. Graphene Based Electrochemical Sensors and Biosensors: A Review. *Electroanalysis*. 2010;22(10):1027-36.
5. Hu C, Lu T, Chen F, Zhang R. A brief review of graphene–metal oxide composites synthesis and applications in photocatalysis. *Journal of the Chinese Advanced Materials Society*. 2013;1(1):21-39.
6. Dong X, Huang W, Chen P. In Situ Synthesis of Reduced Graphene Oxide and Gold Nanocomposites for Nanoelectronics and Biosensing. *Nanoscale Research Letters*. 2010.
7. Frederix F, Friedt J-M, Choi K-H, Laureyn W, Campitelli A, Mondelaers D, et al. Biosensing Based on Light Absorption of Nanoscaled Gold and Silver Particles. *Analytical Chemistry*. 2003;75(24):6894-900.
8. Velikov KP, Zegers GE, van Blaaderen A. Synthesis and Characterization of Large Colloidal Silver Particles. *Langmuir*. 2003;19(4):1384-9.
9. Jana NR, Sau TK, Pal T. Growing Small Silver Particle as

- Redox Catalyst. The Journal of Physical Chemistry B. 1999;103(1):115-21.
10. Kumar R, N. Abraham T, K. Jain S. Silver Nano Particles Impregnated Alumina For The Removal Of Strontium(II) From Aqueous Solution. *Advanced Materials Letters*. 2012;3(6):507-10.
 11. Li Q, Mahendra S, Lyon DY, Brunet L, Liga MV, Li D, et al. Antimicrobial nanomaterials for water disinfection and microbial control: Potential applications and implications. *Water Research*. 2008;42(18):4591-602.
 12. Han K, Miao P, Tong H, Liu T, Cheng W, Zhu X, et al. Preparation of silver nanoparticles/graphene nanosheets as a catalyst for electrochemical oxidation of methanol. *Applied Physics Letters*. 2014;104(5):053101.
 13. Das MR, Sarma RK, Saikia R, Kale VS, Shelke MV, Sengupta P. Synthesis of silver nanoparticles in an aqueous suspension of graphene oxide sheets and its antimicrobial activity. *Colloids and Surfaces B: Biointerfaces*. 2011;83(1):16-22.
 14. Ma J, Zhang J, Xiong Z, Yong Y, Zhao XS. Preparation, characterization and antibacterial properties of silver-modified graphene oxide. *J Mater Chem*. 2011;21(10):3350-2.
 15. Kumar SV, Huang NM, Lim HN, Zainy M, Harrison I, Chia CH. Preparation of highly water dispersible functional graphene/silver nanocomposite for the detection of melamine. *Sensors and Actuators B: Chemical*. 2013;181:885-93.
 16. Hsu K-C, Chen D-H. Microwave-assisted green synthesis of Ag/reduced graphene oxide nanocomposite as a surface-enhanced Raman scattering substrate with high uniformity. *Nanoscale Research Letters*. 2014;9(1).
 17. Mayavan S, Sim J-B, Choi S-M. Easy synthesis of nitrogen-doped graphene-silver nanoparticle hybrids by thermal treatment of graphite oxide with glycine and silver nitrate. *Carbon*. 2012;50(14):5148-55.
 18. Shen J, Shi M, Li N, Yan B, Ma H, Hu Y, et al. Facile synthesis and application of Ag-chemically converted graphene nanocomposite. *Nano Research*. 2010;3(5):339-49.
 19. Li X, Tay BK, Li J, Tan D, Tan CW, Liang K. Mildly reduced graphene oxide-Ag nanoparticle hybrid films for surface-enhanced Raman scattering. *Nanoscale Research Letters*. 2012;7(1).
 20. Nafey AA, Subramanian P, Addad A, Sieber B, Szunerits S, Boukherroub R. Green Synthesis of Reduced Graphene Oxide-Silver Nanoparticles Using Environmentally Friendly L-arginine for H₂O₂ Detection. *ECS Journal of Solid State Science and Technology*. 2016;5(8):M3060-M6.
 21. Pastoriza-Santos I, Liz-Marzán LM. Formation and Stabilization of Silver Nanoparticles through Reduction by N,N-Dimethylformamide. *Langmuir*. 1999;15(4):948-51.
 22. Kuznetsova NP, Ermakova TG, Pozdnyakov AS, Emel'yanov AI, Prozorova GF. Synthesis and characterization of silver polymer nanocomposites of 1-vinyl-1,2,4-triazole with acrylonitrile. *Russian Chemical Bulletin*. 2013;62(11):2509-13.
 23. Ai K, Liu Y, Lu L, Cheng X, Huo L. A novel strategy for making soluble reduced graphene oxide sheets cheaply by adopting an endogenous reducing agent. *J Mater Chem*. 2011;21(10):3365-70.
 24. Cai D, Song M. Preparation of fully exfoliated graphite oxide nanoplatelets in organic solvents. *Journal of Materials Chemistry*. 2007;17(35):3678.
 25. Paredes JI, Villar-Rodil S, Martínez-Alonso A, Tascón JMD. Graphene Oxide Dispersions in Organic Solvents. *Langmuir*. 2008;24(19):10560-4.
 26. Yang Y-K, He C-E, He W-J, Yu L-J, Peng R-G, Xie X-L, et al. Reduction of silver nanoparticles onto graphene oxide nanosheets with N,N-dimethylformamide and SERS activities of GO/Ag composites. *Journal of Nanoparticle Research*. 2011;13(10):5571-81.
 27. Hummers WS, Offeman RE. Preparation of Graphitic Oxide. *Journal of the American Chemical Society*. 1958;80(6):1339-.
 28. Singh VK, Patra MK, Manoth M, Gowd GS, Vadera SR, Kumar N. In situ synthesis of graphene oxide and its composites with iron oxide. *New Carbon Materials*. 2009;24(2):147-52.
 29. Warren BE. X-Ray Diffraction in Random Layer Lattices. *Physical Review*. 1941;59(9):693-8.
 30. Dresselhaus MS, Dresselhaus G, Hofmann M. Raman spectroscopy as a probe of graphene and carbon nanotubes. *Philosophical Transactions of the Royal Society A: Mathematical, Physical and Engineering Sciences*. 2007;366(1863):231-6.
 31. Malard LM, Pimenta MA, Dresselhaus G, Dresselhaus MS. Raman spectroscopy in graphene. *Physics Reports*. 2009;473(5-6):51-87.
 32. Saito R, Hofmann M, Dresselhaus G, Jorio A, Dresselhaus MS. Raman spectroscopy of graphene and carbon nanotubes. *Advances in Physics*. 2011;60(3):413-550.
 33. Guo H-L, Wang X-F, Qian Q-Y, Wang F-B, Xia X-H. A Green Approach to the Synthesis of Graphene Nanosheets. *ACS Nano*. 2009;3(9):2653-9.
 34. Chen C, Chen T, Wang H, Sun G, Yang X. A rapid, one-step, variable-valence metal ion assisted reduction method for graphene oxide. *Nanotechnology*. 2011;22(40):405602.
 35. Tuinstra F, Koenig JL. Raman Spectrum of Graphite. *The Journal of Chemical Physics*. 1970;53(3):1126-30.
 36. Reich S, Thomsen C. Raman spectroscopy of graphite. *Philosophical Transactions of the Royal Society of London Series A: Mathematical, Physical and Engineering Sciences*. 2004;362(1824):2271-88.
 37. Banhart F, Kotakoski J, Krasheninnikov AV. Structural Defects in Graphene. *ACS Nano*. 2010;5(1):26-41.
 38. Caňado LG, Jorio A, Ferreira EHM, Stavale F, Achete CA, Capaz RB, et al. Quantifying Defects in Graphene via Raman Spectroscopy at Different Excitation Energies. *Nano Letters*. 2011;11(8):3190-6.
 39. Ferrari AC, Meyer JC, Scardaci V, Casiraghi C, Lazzeri M, Mauri F, et al. Raman Spectrum of Graphene and Graphene Layers. *Physical Review Letters*. 2006;97(18).
 40. Das A, Pisana S, Chakraborty B, Piscanec S, Saha SK, Waghmare UV, et al. Monitoring dopants by Raman scattering in an electrochemically top-gated graphene transistor. *Nature Nanotechnology*. 2008;3(4):210-5.
 41. Eda G, Lin Y-Y, Mattevi C, Yamaguchi H, Chen H-A, Chen IS, et al. Blue Photoluminescence from Chemically Derived Graphene Oxide. *Advanced Materials*. 2010;22(4):505-9.
 42. Zhu S, Zhang J, Tang S, Qiao C, Wang L, Wang H, et al. Surface Chemistry Routes to Modulate the Photoluminescence of Graphene Quantum Dots: From Fluorescence Mechanism to Up-Conversion Bioimaging Applications. *Advanced Functional Materials*. 2012;22(22):4732-40.
 43. Gan Z, Xiong S, Wu X, Xu T, Zhu X, Gan X, et al. Mechanism of Photoluminescence from Chemically Derived Graphene Oxide: Role of Chemical Reduction. *Advanced Optical*

- Materials. 2013;1(12):926-32.
44. Biroju RK, Rajender G, Giri PK. On the origin and tunability of blue and green photoluminescence from chemically derived graphene: Hydrogenation and oxygenation studies. *Carbon*. 2015;95:228-38.
45. Pal SK. Versatile photoluminescence from graphene and its derivatives. *Carbon*. 2015;88:86-112.
46. Chien C-T, Li S-S, Lai W-J, Yeh Y-C, Chen H-A, Chen IS, et al. Tunable Photoluminescence from Graphene Oxide. *Angewandte Chemie International Edition*. 2012;51(27):6662-6.
47. Gan ZX, Xiong SJ, Wu XL, He CY, Shen JC, Chu PK. Mn²⁺-Bonded Reduced Graphene Oxide with Strong Radiative Recombination in Broad Visible Range Caused by Resonant Energy Transfer. *Nano Letters*. 2011;11(9):3951-6.
48. Wang W, He D, Duan J, Fu M, Zhang X, Wu H, et al. Modulated photoluminescence of graphene quantum dots in the vicinity of an individual silver nano-octahedron. *Physical Chemistry Chemical Physics*. 2014;16(10):4504.
49. Mooradian A. Photoluminescence of Metals. *Physical Review Letters*. 1969;22(5):185-7.
50. Zhao Y, Jiang Y, Fang Y. Spectroscopy property of Ag nanoparticles. *Spectrochimica Acta Part A: Molecular and Biomolecular Spectroscopy*. 2006;65(5):1003-6.